Available online at www.sciencedirect.com
ScienceDirect
Trans. Nonferrous Met. Soc. China 22(2012) 1393−1400
Transactions of Nonferrous Metals Society of China
www.tnmsc.cn

Effects of Cr content on electrochemical properties of melt-spun $Al_{75-x}Si_{25}Cr_x$ alloy anodes for lithium-ion batteries

LIANG Pu, ZHANG Lin-ping, WANG Fei, SUN Zhan-bo, HU Qing, YANG Sen, WANG Li-qun, SONG Xiao-ping

Key Laboratory for Non-equilibrium Synthesis and Modulation of Condensed Matter of Ministry of Education, State Key Laboratory for Mechanical Behavior of Materials, Xi'an Jiaotong University, Xi'an 710049, China

Received 1 April 2011; accepted 10 October 2011

Abstract: Melt-spun $Al_{75-x}Si_{25}Cr_x$ (x=2, 4, 7, 10, mole fraction, %) alloys were investigated as anode materials for lithium-ion batteries. The as-quenched ribbons consist of nano-grains and metallic glass. The electrochemical measurements reveal that an activation behavior is exhibited in the anodes. The specific capacity of the $Al_{73}Si_{25}Cr_2$ anodes can reach a maximum of 1119 mA·h/g and maintain at 586 mA·h/g after 30 cycles. A more stable cycle performance is shown and a capacity loss is only 24% over 30 cycles for $Al_{71}Si_{25}Cr_4$. The intermetallic compounds with Li cannot be detected in the lithiated anodes. After the ribbons were annealed, the specific capacities become much lower due to the formation of inert $Al_{13}Si_4Cr_4$, and an AlLi phase can be tested in the lithiated anodes. The Cr dissolved in the non-equilibrium alloys causes low lithiation activity and strong structure stability, which could be the main reason of the activation and a restriction of structure evolution.

Key words: lithium-ion battery; Al−Si−Cr alloy; melt spinning; electrochemical property; lithiation activity

1 Introduction

Lithium-ion batteries have huge market potential in portable electronic devices and electric vehicles due to their small volume, light weight, high capacity, environmental friendliness, etc. In recent years, research on lithium-ion batteries has been conducted in many fields, such as energy, chemistry and material science. Properties of lithium-ion batteries are significantly affected by anode materials. Currently, graphite is commercially used as an anode material for lithium-ion batteries due to its excellent cycle performance. However, its theoretical specific capacity is low (372 mA·h/g), which could not meet the demand for high-energy lithium-ion batteries.

A series of studies have shown that some semimetals and metals can react with Li to form intermetallic compounds at room temperature, which exhibits high theoretical specific capacities. For example, the specific capacities of $Li_{4.4}Si$, $Li_{2.25}Al$ and $Li_{4.4}Sn$ can reach 4212, 2235 and 990 mA·h/g, respectively [1−3]. However, an obvious structure evolution and a large volume effect can take place in the anodes during lithiation−delithiation processes. This leads to an inevitable pulverization of the materials and a rapid decrease of the capacities. Thus, in order to improve the durability of pure metal anodes, alloy anode materials, especially A−M intermetallic compounds, are widely attempted, where A is the active elements that can react with Li at room temperature, such as Al, Sn, Sb and Si, and M is the inert elements [4−7]. The cyclability would be improved obviously by the addition of the inert component which could alleviate the volume variation during charge−discharge processes. Meanwhile, various synthesis methods, such as ball milling, electrodeposition, magnetron sputtering and melt spinning [8−11], have been adopted to prepare the materials with special structure in order to further improve the cycle behaviors. For example, thin films of Si−Al−M (M=Cr, Fe, Mn, Ni) negative electrode materials were characterized by combinatorial and high-throughput techniques. The results demonstrated that transition metal element and its content had a significant impact on capacity [12]. Ti−Si alloy anode materials prepared by melt spinning, which can prepare non-equilibrium alloys with fine microstructures [13−15], exhibited good cycle performances [16].

In our prior work [17,18], $Al_{70-x}Si_{30}Mn_x$ and $Al_{60-x}Si_{40}Mn_x$ (x=0, 1, 3, 5, 7, 10, mole fraction, %)

Foundation item: Projects (50871081, 51002117, 51071117) supported by the National Natural Science Foundation of China
Corresponding author: SUN Zhan-bo; Tel: +86-29-8266595; Fax: +86-29-83237910; E-mail: szb@mail.xjtu.edu.cn
DOI: 10.1016/S1003-6326(11)61331-9

ribbons were prepared by melt spinning and then studied as anode materials for lithium-ion batteries. Compared with the binary Al−Si anodes, the cycle behaviors of the ternary Al−Si−Mn anodes were improved obviously. Latterly, the effects of alloy state on the electrochemical properties of the Al−Si−Mn alloy anodes were investigated. The results revealed that the cycle behaviors of the melt-spun alloy anodes were better than those of the equilibrium alloys [19]. So, the non-equilibrium state of the Al−Si-based alloys was essential for favorable cycle behaviors. It is worth noting that the high initial specific capacities and the large first irreversible capacities (the capacity differences between the first and the second discharge cycles) were shown in some $Al_{70-x}Si_{30}Mn_x$ and $Al_{60-x}Si_{40}Mn_x$ anodes. Consequently, these anodes presented poor cycle performances. For example, the first discharge specific capacity of the $Al_{59}Si_{40}Mn_1$ anodes could achieve 1803 mA·h/g, but declined to 636 mA·h/g in the next cycle. As a result, a low specific capacity of 125 mA·h/g was shown after 10 cycles. But certain alloy anodes with lower initial specific capacities and less first irreversible capacities exhibited better cycle behaviors compared with $Al_{70-x}Si_{30}Mn_x$ and $Al_{60-x}Si_{40}Mn_x$ anodes. For instance, a stable specific capacity of 500 mA·h/g could be obtained over 10 cycles for the $Al_{53}Si_{40}Mn_7$ anodes. These results manifested that the favorable cycle properties could be obtained by the modulation of the first irreversible capacities. A substitution for the third inert component Mn might be an effective method to obtain better cycle performances.

According to the binary alloy phase diagrams [20], the solubility of Li in Cr is less than that in Mn. In this work, the melt-spun Al−Si−Cr alloys were investigated as anode materials for lithium-ion batteries. As the prior experiments indicated that the α-Si influenced a little on the electrochemical properties of the $Al_{70-x}Si_{30}Mn_x$ and $Al_{60-x}Si_{40}Mn_x$ anodes, lower Si content was adopted for the melt-spun Al−Si−Cr anodes.

2 Experimental

Pure aluminum (99.95%), pure silicon (99.99%) and pure chromium (99.95%) were used to prepare the Al−Si−Cr alloys. The raw materials were arc melted with a non-consumable tungsten electrode under the protection of Ar. The alloy ingots were put into quartz tubes with d 1 mm bottom holes and then heated by high-frequency induction. After being fully melted, they were blown from the bottom holes to a cooling roller to quench into ribbons. The obtained ribbons were about 3 mm in width and 30 μm in thickness. The phase constitutions of the ribbons were analyzed on a Bruker D8 Advance X-ray diffractometer. The thermodynamical state of the as-quenched ribbons was tested on a NETZSCH STA−449C simultaneous thermal analyzer. The microstructures of the ribbons were observed on a JEM−2100 transmission electron microscope (TEM).

The ribbons were grinded into powders, and mixed with carbon black homogenously. Then, the mixture was blended with polyvinylidene fluoride (PVDF) dissolved in N-methylpyrrolidone (NMP) into slurry. The mass ratio of the powders to carbon black to PVDF was 84:8:8. The slurry was evenly coated on a rough copper foil and dried at 373 K in a vacuum oven for 10 h to remove the NMP. Then, the copper foil with the slurry was cut into wafers of d10 mm. The mass of the alloy powders on an anode was about 0.001 g, and the weighing error was ±0.00001 g. Simulation cell was assembled in a dry glove box filled with pure Ar, and the counter electrode was pure lithium. The electrolyte was 1 mol/L $LiPF_6$ in ethylene carbonate (EC)−diethyl carbonate (DEC) (1:1, volume fraction). The electrochemical performance of the electrodes was tested on an Arbin BT−2000 instrument under a constant current density of 65 mA/g. To activate the electrode materials gradually, the lowest cut-off voltages were set to be 0.13 and 0.10 V in the first 2 cycles, respectively, and 0.03 V in the following cycles. The cyclic voltammogram (CV) measurements were conducted on a VersaSTAT MC instrument in the potential region between 0 and 1.0 V (vs Li^+/Li) at a scan rate of 0.2 mV/s. The structures of the anodes after lithiation were analyzed by the X-ray diffraction (XRD) method. The surface morphologies of the anodes experienced 30 cycles were observed on a JSM−7000F scanning electron microscope (SEM). In order to analyze the lithiation mechanism, the melt-spun alloys were annealed at 673 K for 5 h, and the phase constitution, microstructure, electrochemical performance, CV curves of the annealed ribbons and the structure of the lithiated alloys were analyzed.

3 Results

Figure 1 shows the XRD patterns of the as-quenched and annealed $Al_{75-x}Si_{25}Cr_x$ (x=2, 4, 7, 10, mole fraction, %) ribbons. The diffraction peaks of α(Al) and α-Si appear in the pattern of the as-quenched $Al_{73}Si_{25}Cr_2$ ribbons. It is noticeable that only the diffraction peaks of α(Al) can be detected in the as-quenched $Al_{75-x}Si_{25}Cr_x$ ribbons when the Cr contents are in a range of 4%−10%, and the intensity of the α(Al) peaks declines gradually as the Cr contents increase. The lattice parameter of α(Al) is 0.4042 nm for the as-quenched $Al_{73}Si_{25}Cr_2$ and $Al_{71}Si_{25}Cr_4$ ribbons and 0.4044 nm for the $Al_{68}Si_{25}Cr_7$ and $Al_{65}Si_{25}Cr_{10}$. As the as-quenched $Al_{71}Si_{25}Cr_4$ ribbons are annealed, the diffraction peaks of α-Si become much stronger and the

diffraction peaks of $Al_{13}Si_4Cr_4$ appear. The lattice parameter of α(Al) is 0.4050 nm, close to pure Al (0.4049 nm). Typical differential scanning calorimetry (DSC) curves of the as-quenched and annealed $Al_{75-x}Si_{25}Cr_x$ ribbons are exhibited in Fig. 2. Two large exothermal peaks between 400 and 650 K are shown in the curve of the as-quenched ribbons, while they disappear as the ribbons are annealed. This indicates that the as-quenched ribbons are non-equilibrium in thermodynamics and α(Al) is a supersaturated solid solution.

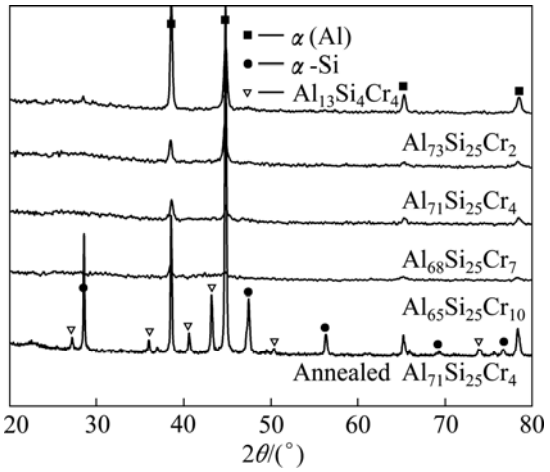

Fig. 1 XRD patterns of as-quenched $Al_{75-x}Si_{25}Cr_x$ and annealed $Al_{71}Si_{25}Cr_4$ ribbons

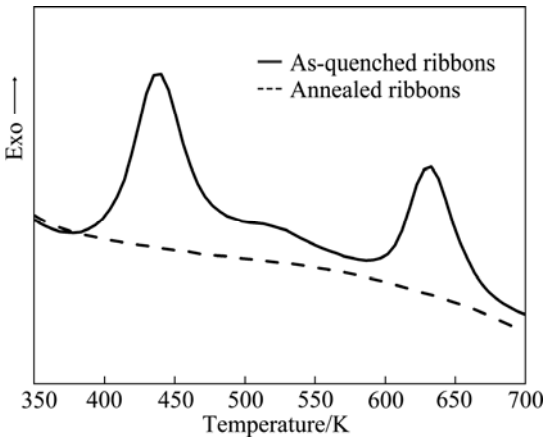

Fig. 2 DSC curves of as-quenched and annealed $Al_{71}Si_{25}Cr_4$ ribbons

The TEM images of the as-quenched and annealed $Al_{75-x}Si_{25}Cr_x$ ribbons are shown in Fig. 3. The as-quenched $Al_{73}Si_{25}Cr_2$ ribbons consist of nano-scale α(Al) grains and a little metallic glass (denoted by the arrows), as seen in Fig. 3(a). For the as-quenched $Al_{71}Si_{25}Cr_4$ ribbons, the sizes of the α(Al) grains (denoted by the ovals), as shown in Fig. 3(b), decrease obviously and the content of the metallic glass increases. After being annealed, the $Al_{71}Si_{25}Cr_4$ ribbons crystallize fully. The grains of α-Si and $Al_{13}Si_4Cr_4$ distribute alternately in the α(Al) matrix and their sizes are about 200 nm, as seen in Fig. 3(c).

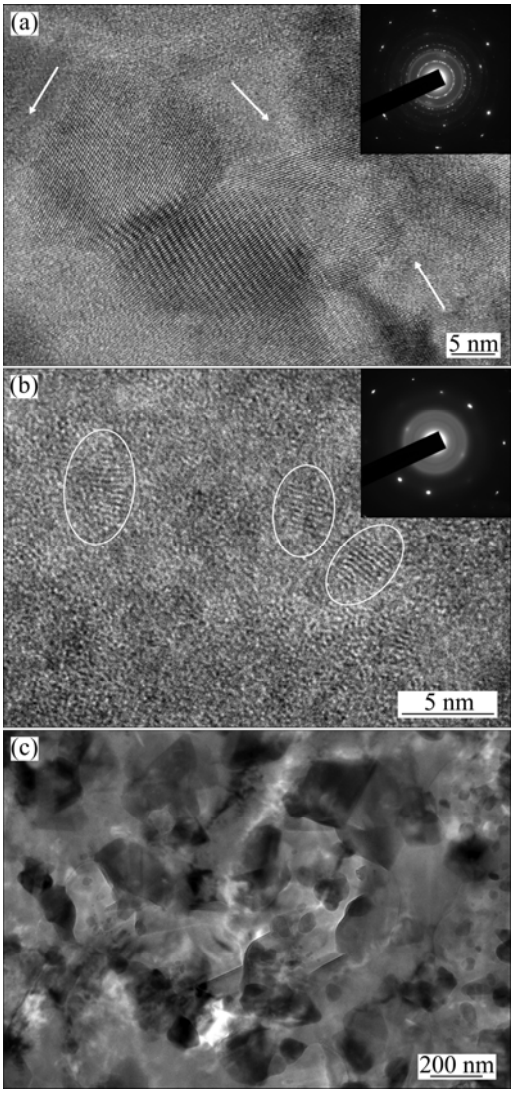

Fig. 3 TEM images of as-quenched $Al_{73}Si_{25}Cr_2$ (a), as-quenched $Al_{71}Si_{25}Cr_4$ (b) and annealed $Al_{71}Si_{25}Cr_4$ (c)

The cycle performance curves of the as-quenched and annealed $Al_{75-x}Si_{25}Cr_x$ alloy anodes are shown in Fig. 4. It is noticed that a low discharge specific capacity of 227 mA·h/g is exhibited in the first cycle for the $Al_{73}Si_{25}Cr_2$ anodes, and 56 mA·h/g in the next cycle. Subsequently, the specific capacity increases to a maximum of 1119 mA·h/g within 6 cycles. In addition, it maintains at 586 mA·h/g after 30 cycles due to the slow fading rate. Before the specific capacity reaches the maximum, the capacity variation of the $Al_{71}Si_{25}Cr_4$ anodes is similar to that of the $Al_{73}Si_{25}Cr_2$. The highest specific capacity of 716 mA·h/g is shown at the 7th cycle, but a capacity loss is only 24% over 30 cycles, exhibiting a more stable cycle performance. As for the $Al_{68}Si_{25}Cr_7$, the specific capacity increases slowly to the largest value

of 240 mA·h/g at the 30th cycle. A low specific capacity of 98 mA·h/g remains stable over 30 cycles for the $Al_{65}Si_{25}Cr_{10}$. After the as-quenched $Al_{71}Si_{25}Cr_4$ alloys are annealed, the specific capacity is 90 mA·h/g at the first cycle and can reach the maximum of 310 mA·h/g at the 7th cycle. It then declines gradually in the following cycles.

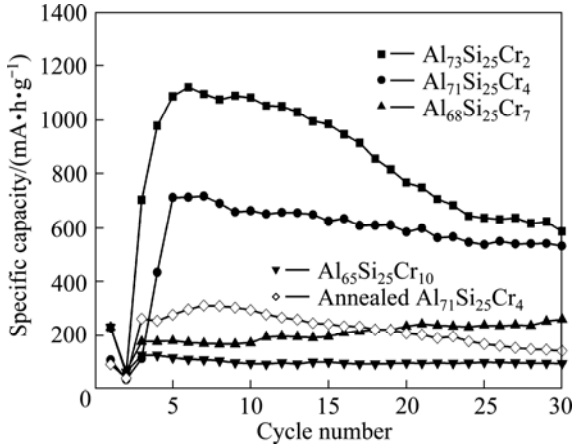

Fig. 4 Cycle performance of as-quenched $Al_{75-x}Si_{25}Cr_x$ and annealed $Al_{71}Si_{25}Cr_4$ anodes

The XRD patterns of the lithiated $Al_{75-x}Si_{25}Cr_x$ (x=2, 4, %) anodes are indicated in Fig. 5. Compared with the ribbons (Fig. 1), new diffraction peaks cannot be detected in the as-quenched alloys after lithiation, indicating that the formation of intermetallic compounds with Li do not occur evidently. However, an AlLi compound can be tested in the lithiated anodes prepared by annealed $Al_{71}Si_{25}Cr_4$ ribbons. These results manifest that the alloy states and phase constitutions have an important influence on the lithiation mechanism.

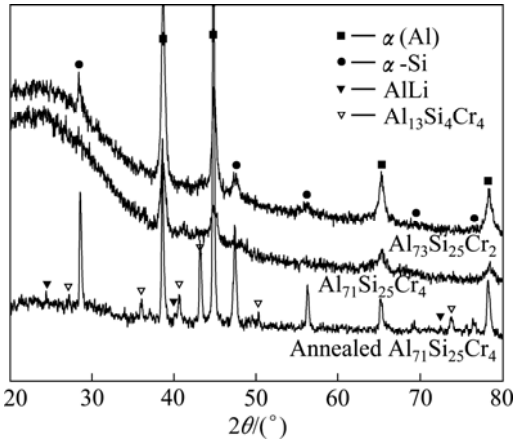

Fig. 5 XRD patterns of as-quenched and annealed $Al_{75-x}Si_{25}Cr_x$ alloys after lithiation

Figure 6 shows the CVs of the as-quenched and annealed $Al_{75-x}Si_{25}Cr_x$ alloy anodes during the first five cycles. The small cathodic current peaks located at about 0.81V and 0.50V at the first cycle, which disappear in the following cycles, are attributed to the reduction of the surface oxides and the formation of SEI film [21]. As for the as-quenched $Al_{73}Si_{25}Cr_2$ and $Al_{71}Si_{25}Cr_4$ anodes, the current value increases gradually with the decline of potential and a cathodic peak cannot be observed evidently, as shown in Figs. 6(a)−(b). The anodic peaks of them exhibit a broad trend. However, an obvious cathodic peak located at about 0.16V appears in the annealed $Al_{71}Si_{25}Cr_4$ anodes, as seen in Fig. 6(c). According to the results of Ref. [22], it can be deduced

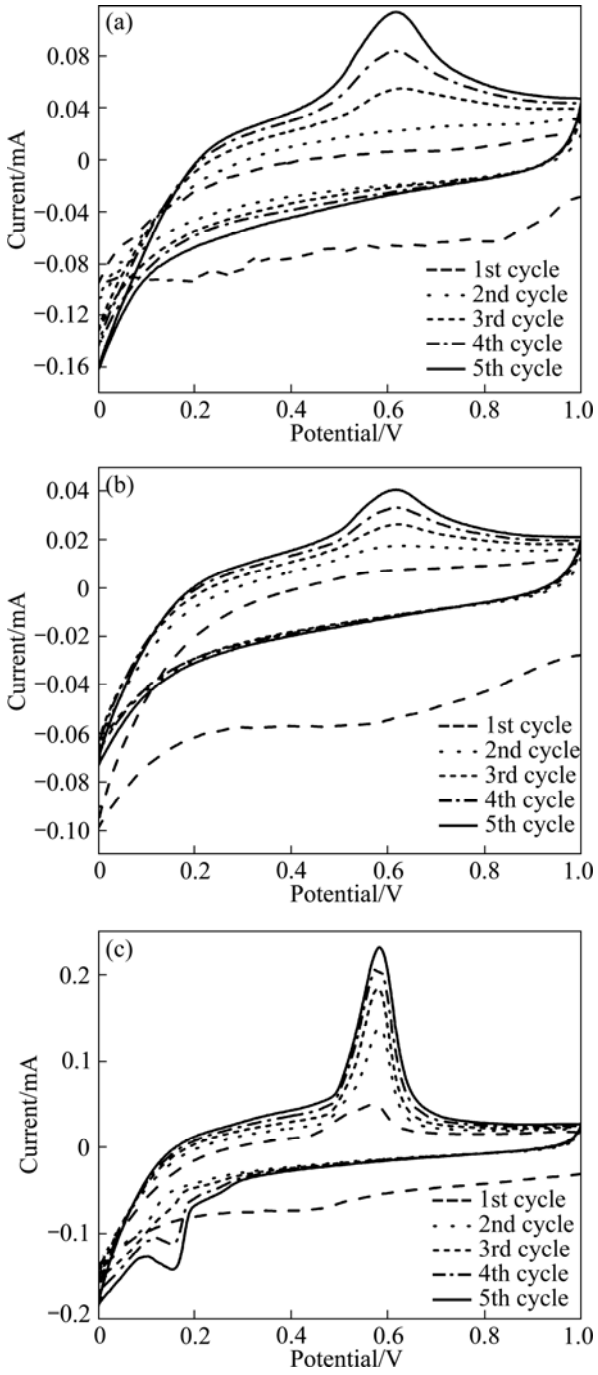

Fig. 6 CVs of as-quenched $Al_{73}Si_{25}Cr_2$ (a), as-quenched $Al_{71}Si_{25}Cr_4$ (b) and annealed $Al_{71}Si_{25}Cr_4$ (c)

that the peak corresponds to the formation of AlLi intermetallic compounds. Accordingly, a sharp anodic peak located at about 0.58 V represents the decomposition of AlLi. These results are consistent with the XRD results of the lithiated $Al_{75-x}Si_{25}Cr_x$ anodes (Fig. 5).

The morphologies of the as-quenched $Al_{75-x}Si_{25}Cr_x$ alloy anodes over 30 charge−discharge cycles are presented in Fig. 7. Cracks and shedding of powders, as indicated in Figs. 7(a)−(b), can be observed in the $Al_{73}Si_{25}Cr_2$ and $Al_{71}Si_{25}Cr_4$ anodes. However, they cannot be seen obviously on the surfaces of the $Al_{68}Si_{25}Cr_7$ and $Al_{65}Si_{25}Cr_{10}$ anodes, seen in Figs. 7(c)−(d), which is attributed to the low capacities.

4 Discussion

The experimental results indicate that the as-quenched $Al_{75-x}Si_{25}Cr_x$ ribbons are non-equilibrium in thermodynamics (Fig. 2). The α(Al) is a supersaturated solid solution and the fraction of the metallic glass increases with the Cr content (Fig. 1). The specific capacities can increase gradually as the cycle continues, and reach the maximum after several cycles, indicating that an activation process is involved during cycle. In particular, the specific capacities of 586 and 544 s mA·h/g can be maintained respectively after 30 cycles for the as-quenched $Al_{73}Si_{25}Cr_2$ and $Al_{71}Si_{25}Cr_4$ anodes, respectively, manifesting that the cycle performance of the as-quenched $Al_{75-x}Si_{25}Cr_x$ anodes has been improved significantly on the basis of high specific capacity compared with as-quenched $Al_{70-x}Si_{30}Mn_x$ and $Al_{60-x}Si_{40}Mn_x$ [17,18]. The intermetallic compounds with Li cannot be detected in the as-quenched $Al_{75-x}Si_{25}Cr_x$ anodes after lithiation (Fig. 5), which is consistent with the as-quenched $Al_{70-x}Si_{30}Mn_x$ and $Al_{60-x}Si_{40}Mn_x$ [17,18]. It can be presumed that the lithium atoms contributing a lot to the high specific capacities are stored in the Al−Si-based supersaturated solid solution and the metallic glass. However, after the $Al_{71}Si_{25}Cr_4$ alloys are annealed, the specific capacities reduce obviously and AlLi compounds appear in the lithiated anodes.

The research of Li storage behavior in metallic glass is less. When the Cr content is increased to 4%, the metallic glass becomes the matrix in the as-quenched alloys (Fig. 3). It can be concluded that the metallic glass can be served as the Li storage phase due to the high capacities of the as-quenched $Al_{71}Si_{25}Cr_4$ alloys (Fig. 4), which also means that the Li atoms can diffuse in the metallic glass. The grain size in the as-quenched alloys is nano-scaled. The area of the interface between α(Al) and the metallic glass increases greatly, and much more Li can store at the interface of the as-quenched alloys. Additionally, the increase of surface tension would increase the solubility of Li in α(Al) and the metallic glass. Thus, high specific capacities can be obtained in the as-quenched $Al_{73}Si_{25}Cr_2$ and $Al_{71}Si_{25}Cr_4$ anodes. However, the Cr dissolved in the alloys will cause an activity decrease for Li storage. When the Cr content is excess (7% and 10%), the Li storage ability would decrease and the specific capacities would reduce.

When the Li atoms are inserted into the alloys, two

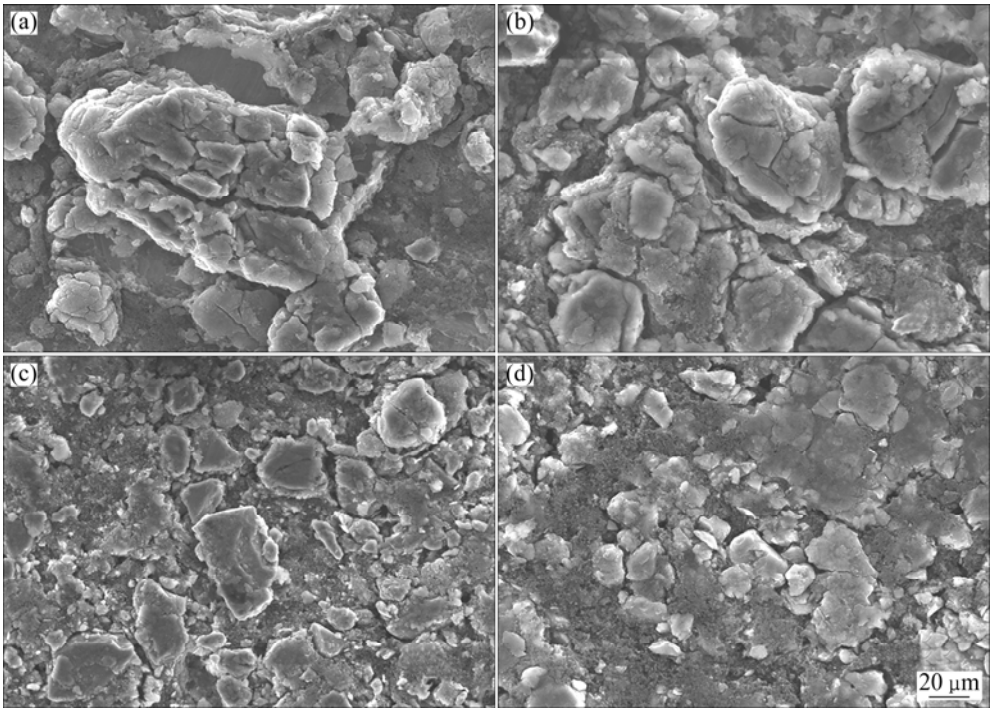

Fig. 7 SEM images showing morphologies of as-quenched $Al_{75-x}Si_{25}Cr_x$ alloy anodes after 30 cycles: (a) $Al_{73}Si_{25}Cr_2$; (b) $Al_{71}Si_{25}Cr_4$; (c) $Al_{68}Si_{25}Cr_7$; (d) $Al_{65}Si_{25}Cr_{10}$

patterns exist possibly. One possibility is that the Li atoms dissolve in the solid solution and metallic glass, the other is that the Li atoms form intermetallic compounds with Al or Si. Figure 5 shows that the formation of Al−Si−Cr compounds or the compounds with Li does not occur during lithiation for the as-quenched alloys. This manifests that the lithiation process would not lead to the crystallization of the metallic glass and the separation of the supersaturated solid solution, indicating that the as-quenched alloys are relatively stable for lithiation. The formation of an intermetallic compound has to meet a strict composition requirement. It could be concluded that the composition requirement cannot be met due to the strong stability of the alloys consisted of the supersaturated solid solution and metallic glass during lithiation. Consequently, a lot of compounds with Li do not appear in the lithiated anodes for the as-quenched alloys. After being annealed, the metallic glass crystallizes, the size of the grains increases, the $Al_{13}Si_4Cr_4$ compounds form and the volume fraction of α(Al) reduces evidently (Fig. 1). It can be confirmed that the $Al_{13}Si_4Cr_4$ compounds are inert for Li storage because the specific capacities of the annealed $Al_{71}Si_{25}Cr_4$ alloys are much lower than those of the as-quenched alloys (Fig. 4). The Si and Cr contents in the Al-based solid solution decrease obviously for the annealed alloys. Thus, the composition requirement and the lattice re-arrangement ability of the AlLi compounds can be met and AlLi can be detected in the annealed anodes after lithiation (Fig. 5). However, the formation of AlLi causes a larger volume expansion and it would be limited because the α(Al), α-Si and $Al_{13}Si_4Cr_4$ co-exist in the annealed alloys. As a result, the fraction of AlLi in the lithiated anodes prepared by the annealed alloy is little. The separation of AlLi is more difficult during Li extraction because of the lower Gibbs free energy of the compound compared with the solution, which could cause more dead Li during cycles. As a result, the cycle properties would be poor when AlLi compounds form during lithiation. Therefore, the favorable electrochemical properties obtained in the non-equilibrium alloys with optimal composition contribute that two Li storage phases of nano-scale α(Al) and the metallic glass co-exist in the as-quenched $Al_{75-x}Si_{25}Cr_x$ alloys. But the volume fraction of the Li storage phases decreases obviously as the non-equilibrium alloys transform to equilibrium state, and the specific capacities decrease clearly in the annealed alloy anodes consequently. So, the alloys in non-equilibrium state are necessary to obtain favorable electrochemical properties.

In the present experiment, the lower initial specific capacities of the $Al_{75-x}Si_{25}Cr_x$ anodes manifest less initial lithiation activity compared with the $Al_{70-x}Si_{30}Mn_x$ and $Al_{60-x}Si_{40}Mn_x$ [17,18]. The difference of atomic radii between Mn and Cr may be an important factor that influences the initial lithiation activity. The radii of Al, Mn, Cr and Li are 0.182, 0.179, 0.185 and 0.205 nm, respectively. For the Al−Si-based supersaturated solid solution, the lattice parameter around Cr atoms would increase, but Mn acts contrarily. When Li atoms with large atomic radius insert into the alloys, the lattice parameter around Cr atoms becomes even larger. For the metallic glass, this effect is similar although the atoms are in short-range order. So, the solubility of Li in the as-quenched $Al_{75-x}Si_{25}Cr_x$ alloys might be less than that in the as-quenched $Al_{70-x}Si_{30}Mn_x$ or $Al_{60-x}Si_{40}Mn_x$ during the first several cycles. Because the Li atoms have to substitute some atomic sites of the parent alloys during lithiation and the sites would become vacancies after the Li atoms are extracted, the sites employed for the Li storage in the alloys increase as the alloys experience several cycles, resulting in the gradual activation of the materials. After being fully activated, the powders can be employed effectively and the highest specific capacities can be reached. The lower lithiation activity of the alloys with high Cr contents (7% and 10%), the more cycles of activation are needed. Thus, the specific capacities of the as-quenched $Al_{68}Si_{25}Cr_7$ and $Al_{65}Si_{25}Cr_{10}$ anodes increase with increasing cycles in the present experiment (Fig. 4). Generally, a system with multi-component can enlarge the inter-solubility among the components. The activation process still exists after the as-quenched alloys are annealed, but it will finish experiencing less cycles because the contents of Si and Cr dissolved in the α(Al) decrease.

Some cracks can be observed in the anodes experiencing 30 cycles because the volume effect is inevitable during the charge−discharge processes (Fig. 7). Since the specific capacities of the $Al_{73}Si_{25}Cr_2$ anodes are the highest among the $Al_{75-x}Si_{25}Cr_x$ anodes, the volume expansion is the most severe. As the capacity retention rate after 30 cycles is 53% of the highest specific capacity, it is a good reason to believe that the fading of the specific capacity is partly ascribed to the powders shedding caused by the large volume expansion. The appropriate activity can limit the overlarge volume expansion, which is beneficial for the cycle behaviors. This effect is consistent with the $Al_{70-x}Si_{30}Mn_x$ and $Al_{60-x}Si_{40}Mn_x$ anodes [17,18]. For instance, the $Al_{53}Si_{40}Mn_7$ anodes exhibit better cycle performance compared with $Al_{70-x}Si_{30}Mn_x$ or $Al_{60-x}Si_{40}Mn_x$ anodes due to their low initial specific capacity and small first irreversible capacity.

The improvement on the electrochemical properties can be attributed to the lower initial specific capacities and special microstructures. The electrochemical properties of the melt-spun Al−Si-based alloy anode

materials can be modulated by the lithiation activity. The skillful adoption of transition metal element and careful control of its concentration could be an effective method to obtain better electrochemical properties.

5 Conclusions

1) Melt-spun $Al_{75-x}Si_{25}Cr_x$ (x=2, 4, 7, 10, mole fraction, %) alloys were studied as anode materials for lithium-ion batteries. Low initial specific capacities are shown and the activation process is involved in the first several cycles. Subsequently, low capacity fading rate is exhibited in the following cycles. The specific capacities of 586 and 544 mA·h/g can be exhibited over 30 cycles for the as-quenched $Al_{73}Si_{25}Cr_2$ and $Al_{71}Si_{25}Cr_4$ anodes, respectively. But the specific capacities decline greatly when the Cr contents are 7% and 10%, respectively.

2) The compounds with Li have not been detected in the lithiated anodes prepared by the as-quenched alloys. Both the supersaturated solid solution of Si and Cr in α(Al) and the metallic glass can store Li, and they are stable during lithiation, resulting in the activation and preventing the compounds with Li from formation.

3) Excessive specific capacity and volume expansion can be limited in the alloys with an appropriate Cr content. The present results predict that the lithiation activity could be modulated by the Cr contents and alloy states, and favorable electrochemical performance can be achieved in some non-equilibrium $Al_{75-x}Si_{25}Cr_x$ alloys.

References

[1] CHO J. Porous Si anode materials for lithium rechargeable batteries [J]. Journal of Materials Chemistry, 2010, 20: 4009−4014.

[2] CHEN Zhong-xue, QIAN Jiang-feng, AI Xin-ping, CAO Yu-liang, YANG Han-xi. Electrochemical performances of Al-based composites as anode materials for Li-ion batteries [J]. Electrochimica Acta, 2009, 54(16): 4118−4122.

[3] AIFANTIS K E, BRUTTI S, HACKNEY S A, SARAKONSRI T, SCROSATI B. SnO_2/C nanocomposites as anodes in secondary Li-ion batteries [J]. Electrochimica Acta, 2010, 55(18): 5071−5076.

[4] HOU Xian-hua, YU Hong-wen, HU She-jun. Preparation and properties of Sn−Al thin-film electrode material for lithium ion batteries [J]. Acta Physica Sinica, 2010, 59(11): 8226−8230.

[5] HUANG Ke-long, ZHANG Ge, LIU Su-qin. Effect of graphite content on electrochemical performance of Sn−SnSb/graphite composite powders [J]. Transactions of Nonferrous Metals Society of China, 2007, 17(4): 841−845.

[6] PARK C M, SOHN H J. Electrochemical characteristics of $TiSb_2$ and Sb/TiC/C nanocomposites as anodes for rechargeable Li-ion batteries [J]. Journal of the Electrochemical Society A, 2010, 157(1): 46−49.

[7] PARK S E, KIM B E, LEE S W, LEE J K. Employment of encapsulated Si with mesoporous TiO_2 layer as anode material for lithium secondary batteries [J]. Transactions of Nonferrous Metals Society of China, 2009, 19(4): 1023−1026.

[8] JIANG Xiao-bing, ZHAO Xin-bing, ZHANG Xiao-bin, ZHANG Li-juan, CAO Gao-shao, ZHOU Bang-chang. Lithium-ion-storage behaviors of $CoSb_3$ intermetallic compound and effects of some carbonaceous additives [J]. Transactions of Nonferrous Metals Society of China, 2001, 11(6): 852−855.

[9] HUANG Ling, CAI Jin-shu, HE Yang, KE Fu-sheng, SUN Shi-gang. Structure and electrochemical performance of nanostructured Sn−Co alloy/carbon nanotube composites as anodes for lithium ion batteries [J]. Electrochemistry Communications, 2009, 11(5): 950−953.

[10] HWANG C M, PARK J W. Electrochemical characterization of a Ge-based composite film fabricated as an anode material using magnetron sputtering for lithium ion batteries [J]. Thin Solid Films, 2010, 518(22): 6590−6597.

[11] ZHANG Shu-kai, SHU Kang-ying, LEI Yong-quan, LU Guang-lie, WANG Qi-dong. Phase structure and electrochemical properties of melt-spinning alloy Zr(MnVNi)(2.4) [J]. Transactions of Nonferrous Metals Society of China, 2003, 13(4): 926−929.

[12] FLEISCHAUER M D, OBROVAC M N, DAHN J R. Simple model for the capacity of amorphous silicon-aluminum-transition metal negative electrode materials [J]. Journal of the Electrochemical Society A, 2006, 153(6): 1201−1205.

[13] ZHANG Yang-huan, ZHAO Dong-liang, SHI Yan-chun, QI Yan, HUO Shi-hai, WANG Xin-lin. Structures and electrochemical performances of $La_{0.75-x}Zr_xMg_{0.25}Ni_{3.2}Co_{0.2}Al_{0.1}$ (x=0−0.2) electrode alloys prepared by melt spinning [J]. Transactions of Nonferrous Metals Society of China, 2010, 20(4): 607−613.

[14] WANG You-hong, SONG Xiao-ping, SUN Zhan-bo, ZHOU Xuan, GUO Juan. Effects of Ti addition on microstructures of melt-spun CuCr ribbons [J]. Transactions of Nonferrous Metals Society of China, 2007, 17(1): 72−76.

[15] SHU Kang-ying, ZHANG Shu-kai, LEI Yong-quan, ZHANG Hong, WANG Qi-dong. Relationship between cooling rate and electrochemical performance of melt-spun AB(5) alloy [J]. Transactions of Nonferrous Metals Society of China, 2003, 13(4): 922−925.

[16] LEE Y S, LEE J H, KIM Y W, SUN Y K, LEE S M. Rapidly solidified Ti−Si alloys/carbon composites as anode for Li-ion batteries [J]. Electrochimica Acta, 2006, 52(4): 1523−1526.

[17] SUN Zhan-bo, WANG Xiao-dong, LI Xue-peng, ZHAO Ming-shu, LI Yan, ZHU Yao-min, SONG Xiao-ping. Electrochemical properties of melt-spun Al–Si–Mn alloy anodes for lithium-ion batteries [J]. Journal of Power Sources, 2008, 182: 353−358.

[18] SUN Zhan-bo, LI Xue-peng, WANG Xiao-dong, HU Qing, ZHAO Ming-shu, ZHU Yao-min, LI Yan, SONG Xiao-ping. Melt-spun $Al_{70-x}Si_{30}Mn_x$ (x=0, 3, 5, 7, 10) anode in lithium-ion batteries [J]. Science in China Series E, 2009, 52(8): 2288−2294.

[19] LI Qian, HU Qing, SUN Zhan-bo, LI Xue-peng. Separation of $Al_{70-x}Si_{30}Mn_x$ (x=0, 3, 7) supersaturated solid solutions during annealing and its effect on electrochemical property [J]. The Chinese Journal of Nonferrous Metals, 2010, 20(10): 1998−2002. (in Chinese)

[20] OKAMOTO H. Phase diagrams for binary alloys [M]. ASM International, 2000.

[21] CHEN L B, XIE J Y, YU H C, WANG T H. Si–Al thin film anode material with superior cycle performance and rate capability for lithium ion batteries [J]. Electrochimica Acta, 2008, 53: 8149−8153.

[22] HAMON Y, BROUSSE T, JOUSSE F, TOPART P, BUVAT P, SCHLEICH D M. Aluminum negative electrode in lithium ion batteries [J]. Journal of Power Sources, 2001, 97−98: 185−187.

Cr 含量对熔体快淬 $Al_{75-x}Si_{25}Cr_x$ 锂离子电池合金负极电化学性能的影响

梁 普，张林萍，汪 飞，孙占波，胡 青，杨 森，王力群，宋晓平

西安交通大学 物质非平衡合成与调控教育部重点实验室，
金属材料强度国家重点实验室，西安 710049

摘 要：研究熔体快淬 $Al_{75-x}Si_{25}Cr_x$(x=2，4，7，10，摩尔分数，%)锂离子电池合金负极材料的电化学性能。快淬带由纳米晶和非晶组成。电化学测试表明：负极材料存在活化过程；$Al_{73}Si_{25}Cr_2$ 负极材料的最大比容量为 1119 mA·h/g，循环 30 次后可保持为 586 mA·h/g；$Al_{71}Si_{25}Cr_4$ 合金的循环性能更加稳定，经过 30 次循环后，容量仅衰减 24%；嵌 Li 极片中未检测到含 Li 的金属间化合物；退火后，由于惰性相 $Al_{13}Si_4Cr_4$ 的形成，合金的比容量减小，嵌 Li 极片中出现 AlLi 相；固溶于非平衡态合金中的 Cr 降低了嵌 Li 活性，增强了结构稳定性，这是活化和抑制结构演变的主要原因。

关键词：锂离子电池；Al−Si−Cr 合金；熔体快淬；电化学性能；嵌 Li 活性

(Edited by LI Xiang-qun)